Tikrit Journal of Pure Science Vol. 31 (1) 2026

DOI:https://doi.org/10.25130/tjps.v31i1.1878

IRAQI Academic Scientific Journals

Tikrit Journal of Pure Science

ISSN: 1813 – 1662 (Print) --- E-ISSN: 2415 – 1726 (Online)

Journal Homepage: https://tjpsj.org/

Tikrit Journal of Pure Science

Efficiency of Hydrogenated Amorphous Silicon Solar Cells Formed by Grooves in Two Dimensions

Shaema'a Kader Esmaee[1] , Bassam Mahmood Mustafa [2]

[1]*Department of Nursing, College of Nursing, University of Nineveh-Iraq*

[2]*Department of Physics, College of Science, University of Mosul-Iraq*

Received: 24 Jan. 2025 **Received in revised forum:** 7 Apr. 2025 **Accepted:** 14 Apr. 2025

Final Proofreading: 13 Jul. 2025 **Available online:** 25 Feb. 2026

ABSTRACT

In this study, we conducted a theoretical analysis of the effects of grooves on the properties of amorphous silicon solar cells. The studied groove structure consists of prisms arranged perpendicularly to the one-dimensional grooves, and we refer to this formation as the two-dimensional groove. The groove apex angles under investigation are acute, right, and obtuse (40°, 90°, and 110°, respectively). A theoretical method is proposed to calculate the increase in photocurrent resulting from texturing-induced enhanced optical absorption. This is done by analyzing the characteristic equation to find the I-V characteristic for all groove angles. The reflectivity was estimated from the spectral reflectance of a-Si: H, whereas our study focuses on Mosul city in July, when incident solar irradiance is at its peak. The incident solar power, the output power, and the efficiency were determined for each case. Using all the above steps, the input, output and the efficiency are calculated. An increase in efficiency was observed for two-dimensional texturing when the angles are right and obtuse. Also, the prisms arranged perpendicularly will absorb (in the case of one-dimensional), which is common for the early and late hours of the day. The role of the second dimension decreases as normal incidence is approached and becomes zero at normal incidence. The two-dimensional texturing absorbed the escaped energy in the case of one dimension for all groove angles.

Keywords: Two-dimensional texturing, Groove, Amorphous silicon, Spectral reflectance.

Name: Shaema'a Kader Esmaee **E-mail:** shaiemma.qader@uoninevah.edu.iq

Tikrit Journal of Pure Science Vol. 31 (1) 2026

DOI:https://doi.org/10.25130/tjps.v31i1.1878

كفاءة الخلايا الشمسية السليكونية العشوائية المهدرجة المتشكلة بأخاديد ذات بعدين

شيماء قادر اسماعيل[1]، بسام محمود مصطفى[2]

[1]قسم التمريض، كلية التمريض، جامعة نينوى، العراق

[2]قسم الفيزياء، كلية العلوم، جامعة الموصل، العراق

الملخص

في هذا البحث قمنا بدراسة نظرية حول تأثير الأخاديد (Grooves) على خواص الخلايا الشمسية السيليكونية العشوائية والأخدود قيد الدراسة بشكل مواشير متعامدة على الاخاديد ذات البعد الواحد وأسمينا هذا التشكيل بالأخدود ذي البعدين علماً أن زوايا رأس الأخدود تكون حادة وقائمة ومنفرجة (40°, 90°, 110°) تم إيجاد طريقة نظرية لحساب الزيادة في التيار الضوئي الناتج عن زيادة الطاقة الضوئية المقتنصة نتيجة التشكيل من خلال التحليل لمعادلة الخواص لهذا النوع من الخلايا وإيجاد خواص التيار– الفولتية (I-V) لجميع زوايا رأس الأخدود ولزوايا سقوط مختلفة، كما استخدمنا طريقة لحساب قيمة الانعكاسية للخلايا الشمسية السيليكونية العشوائية. حيث تمت الحسابات في شهر تموز لمدينة الموصل بسبب وصول اشعة الشمس لذروتها، وقد حسبت على هذا الأساس مقدار القدرة الشمسية الساقطة للأخاديد الثلاثة والقدرة المحصلة وكذلك الكفاءة. وجد أنه عندما تكون زاوية رأس الأُخدود قائمة ومنفرجة فأن اللوح الشمسي يعمل بكفاءة عالية، وفي حالة التشكيل ببعدين تمتص الطاقة المتبددة (للأشعة في حالة الأخدود ذي البعد الواحد) وهي حالة بارزة في الساعات الأولى والأخيرة للنهار وتقل مساهمة البعد الثاني كلما اقتربنا من السقوط العمودي لتصبح صفراً عندما يكون السقوط عمودياً. ويعمل الأخدود ببعدين على امتصاص الطاقة المتبددة لحالة البعد الواحد ولجميع زوايا رأس الاخدود.

INTRODUCTION

The most promising technologies are those that harness solar energy, as the thermal conversion of solar radiation into electrical energy via solar cells represents an advanced, strategic industry. In the future, solar energy will be regarded as a top priority for humanity, even surpassing water and food. Its widespread adoption will play a crucial role in conserving traditional energy sources for more essential and valuable applications. Moreover, solar energy is abundant, inexhaustible, free, and produces no waste or associated risks.[1, 2]. The depletion of conventional energy sources due to excessive consumption, along with the challenges posed by pollution and global warming, has driven scientists to develop solar cells. [3]. Their objective is to enhance conversion efficiency to meet global energy demands while reducing environmental pollution caused by oil and its derivatives.[4]. In this research, we focus on improving amorphous silicon (a-Si: H) solar cells, given their simpler manufacturing process and lower production costs compared to those of crystalline silicon solar cells. We have selected a development approach that aligns with available resources. The study aims to investigate the impact of grooves on the current-voltage (I-V) characteristics, power output, and overall efficiency of solar cells. This is achieved by incorporating two-dimensional grooves into the cell's base, forming a pyramidal texture that helps reduce surface reflections. The research is conducted during the summer in Mosul, with calculations based on the optimal positioning of solar panels, naturally oriented southward, to maximize efficiency and solar energy absorption.

MATERIALS AND METHODS

We will focus on a type of high-performance solar cells (a-Si: H) with an efficiency of about (10 %) [5]. In general, this cell has an energy gap of about 2 eV

DOI:https://doi.org/10.25130/tjps.v31i1.1878

[6]. Its conversion efficiency is calculated by measuring the current-voltage (I-V) characteristics at the maximum power point ($P_m = J_m\ V_m$), where (Jm, Vm) are the maximum current density and maximum voltage, respectively. Therefore, the conversion efficiency is given by equation [6].

$$\eta = \frac{J_m V_m}{P_m} \quad \dots (1)$$

When Pm represents the incident power, it is important to note that the performance characteristics of different types of solar cells vary with several factors, including structural design and manufacturing processes.

Based on the energy band diagram of the p-i-n structure [7] shown in Figure 1, the photocurrent density can be expressed as follows:

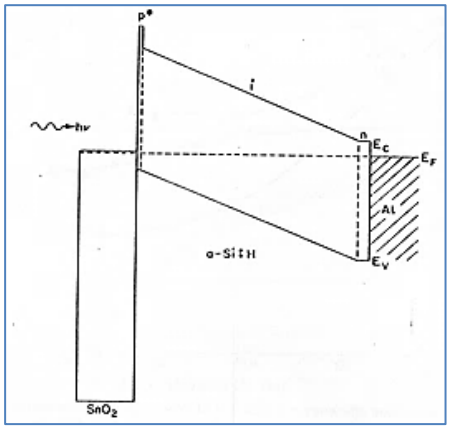

Fig. 1: Energy band diagram of a p-i-n cell in short circuit mode[8].

$$J = qGl_c[1 - \exp(-d/l_c)] \quad \dots (2)$$

Where d is the thickness of the layer (i), and l_c Total drift lengths of electron and hole can be written as follows. [9]:

$$l_c = \mu_n t_n \varepsilon + \mu_p t_p \varepsilon \quad \dots (3)$$

$$G(\lambda) = \alpha(\lambda) N(\lambda)[1 - R(\lambda)] \exp(-\alpha(\lambda) x) \quad \dots (4)$$

Where G is the electron-hole pair generation rate, $\alpha(\lambda)$ represents the absorption coefficient, $N(\lambda)$ represents the photocurrent, and $R(\lambda)$ is the reflection coefficient for a given wavelength. The general structure of this type of solar cell (a-Si: H) consists of two junctions connected by a photovoltaic layer (i). The following equation gives the total current density JT [6]:

$$J_T = J_p - J_d \quad \dots (5)$$

Where as J_d the diffusion current density and J_p is the photocurrent density, which can be expressed as follows:

$$J_d = \frac{nql}{\tau_n} \quad \dots (6)$$

Where (τ_n, q, n) is the density, charge, and relaxation time of electrons in the (i) layer. Therefore, the current-voltage (I-V) characteristics can be described by the equation. [8]:

$$V = -R_c J_T - \frac{V_s(1-0.5\sqrt{J_T/J_p})}{\frac{J_T}{J_{p-1}}} - \frac{\beta kT}{q} \ln\left(1 - \frac{J_T}{J_p}\right)^{-1} + V_{oC} \quad \dots (7)$$

V_s represents the voltage in the (i) layer, R_c is the series ohmic resistance, and β is the ideality factor. It was found that the above equation agrees well with the experimental results. [6]. To calculate the photocurrent density from equation (7), we will do the following: in the case of a short circuit, then: V= 0

$$0 = -R_c J_T - \frac{V_s\left(1-0.5\sqrt{J_T/J_p}\right)}{J_p/J_T - 1} - \frac{\beta kT}{q} \ln(1 - \frac{J_T}{J_p})^{-1} + V_{oc} \quad \dots (8)$$

We reformulate equation (8) as follows:

$$R_c J_T + \frac{V_s\left(1-0.5\sqrt{J_T/J_p}\right)}{J_p/J_T - 1} = \frac{\beta kT}{q} \ln\left(1 - \frac{J_T}{J_p}\right) + V_{oc} \quad \dots (9)$$

To solve J_T $\left(\ln\left(1 - \frac{J_T}{J_p}\right)\right)$ we will have $\left(\frac{J_T}{J_p} \cong 1\right)$ then:

$$\ln(1 - X) = -X - \frac{X^2}{2} - \frac{X^3}{3} + \cdots \quad \dots (10)$$

$$\ln\left(1 - \frac{J_T}{J_p}\right) \cong -\frac{J_T}{J_p} - \frac{1}{2} - \frac{1}{3} \quad \dots (11)$$

$$R_c J_T + \frac{V_s\left(1-0.5\sqrt{J_T/J_p}\right)}{J_p/J_T - 1} = \frac{\beta kT}{q}\left(-\frac{J_T}{J_p} - \frac{1}{2} - \frac{1}{3}\right) = V_{oc} \quad \dots (12)$$

Whereas $\sqrt{J_T}/J_p \cong 1$ then:

$$R_c J_T + \frac{0.5 V_s}{J_p/J_T - 1} = \frac{\beta kT}{q}\left(-\frac{J_T}{J_p} - \frac{1}{2} - \frac{1}{3}\right) + V_{oc} \quad \dots (13)$$

DOI:https://doi.org/10.25130/tjps.v31i1.1878

suppose: $C_2 = \frac{J_T}{J_P}, C_1 = \frac{\beta kT}{q}$

$$R_C J_T + \frac{0.5V_s}{1/C_2 - 1} = C_1\left(-C_2 - \frac{1}{2} - \frac{1}{3}\right) + V_{oc} \quad \ldots (14)$$

$$c_1 c_2^2 + \left[-\frac{1}{6}C_1 + V_{oc} - 0.5V_s + R_C J_T\right] C_2 + V_{oc} - R_C J_T - \frac{5}{6}c_1 = 0 \quad \ldots (15)$$

Equation (15) is a quadratic equation and can be solved as follows:

$$C_2 = \frac{-B \pm \sqrt{B^2 - 4AC}}{2A} \quad \ldots (16)$$

So: $A = c_1, B = \left[-\frac{1}{6}c_1 + V_\alpha - 0.5V_s + R_C J_T\right], C = V_\alpha - R_C J_T - \frac{5}{6}c_1$

Subtitle the value of V_{oc}, V_s, R_C, β, k, q, $and\ T$. We can determine the value of JT for any Jp to introduce modulation. We combine equations (2) and (4), the photocurrent density Jp is as follows:

$$J_p = q l_c \alpha(\lambda) N(\lambda)[1 - R(\lambda)](exp)(-\alpha(\lambda)x)\left[1 - \exp\left(-d/l_c\right)\right] \quad \ldots (17)$$

The impact of shaping primarily results from a reduction in R (i.e., the reflection coefficient decreases).

$$J_p = c_3[1 - R(\lambda)] \quad \ldots (18)$$

Whereas: $c_3 = q l_c \alpha(\lambda) N(\lambda)(exp - \alpha(\lambda)x)\left[1 - \exp\left(-d/l_c\right)\right]$

So if J_{p1}, R_1 represent the photocurrent density and reflection coefficient before shaping, respectively, then, J_{p2}, R_2 represent the photocurrent density, reflection coefficient after shaping, then:

$$J_{p2}/J_{p1} = [1 - R_2]/[1 - R_1] \quad \ldots (19)$$

In the above equation to calculate the photocurrent density after shaping, the photocurrent density before shaping and the reflectivity can be used. [6].

To analyze the effect of shaping on the photocurrent density (Jp) in the plane of incidence, the key parameters are the groove angle and the incidence angle. When light strikes a specific groove, the incident light energy depends on the incidence angle (i), as shown in Figure 2. For incidence angles greater than angle (2), a portion of the groove with length x will be illuminated from the total groove edge length (E) [6].

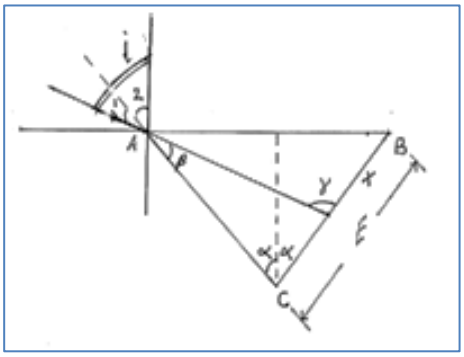

Fig. 2: Geometry of light incidence at angle (i)[6].

Based on the geometry shown in Figure 2 and the triangle's properties, we can apply trigonometric relations.

$$\angle i = \angle 1 + \angle 2;\ \angle\beta = \angle 1;\ \angle\gamma = \angle\beta + 2\angle\alpha \quad \ldots (20)$$

$$\sin\alpha = \frac{OB}{CB} \quad \ldots (21)$$

$$OB = E\sin\alpha \ ;\ AB = 2E\sin\alpha$$ [6].

To find the length of the illuminated part (X), we will use the law of sines.

$$\frac{AB}{\sin\gamma} = \frac{x}{\sin(90 - i)} \quad \ldots (22)$$

By using equations (20) and (21) and substituting them into equation (22), we obtain the following equation:

$$\frac{x}{\cos i} = \frac{2E\sin\alpha}{\sin(i - \alpha)} \quad \ldots (23)$$

In the case of direct incidence of light rays within the groove, either all or a part of the incident rays may be reflected, as shown in Figure 3. [6].

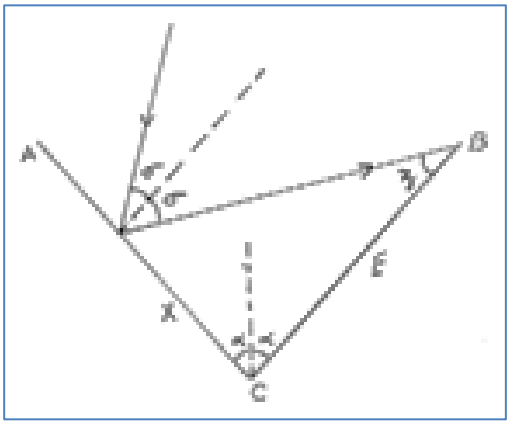

Fig. 3: The geometry of the direct incidence of light rays on the groove [6].

DOI:https://doi.org/10.25130/tjps.v31i1.1878

Reflectivity Calculation

One key aspect of this research is determining the amount of light energy reflected from the solar cell's surface. Since reflectivity changes with wavelength, it was necessary to determine the amount of light energy reflected across all positive wavelengths. To determine the total reflected energy, it is crucial to evaluate the spectral reflectance across all relevant wavelengths in the solar spectrum. We found a study that measured cell reflectance at different wavelengths.[10]. Based on this, we developed a method to calculate the solar energy reflected when the solar spectrum AM1.5 is incident. The reflectivity values for the wavelengths used to calculate the power were compiled, with each wavelength listed along with the incident power.[7]. By applying equations (24) and (25), the total power reflected from amorphous silicon solar cells was computed by averaging two variables, similar to the calibration process in quantum mechanics. This was done by dividing the spectrum into small segments and calculating the average reflectivity for the corresponding wavelengths within each segment.

$$R = \frac{\Sigma(p_1+p_2+p_3+\cdots+p_n)\times(R_1+R_2+R_3+\cdots+R_n)}{\Sigma(p_1+p_2+p_3+\cdots+p_n)} \quad \ldots (24)$$

$$R = \frac{\Sigma p_i \times R_i}{\Sigma p_i} \quad \ldots (25)$$

p_i Is the incident solar power and $R_i$represents the incident solar reflective [6]. To calculate the reflectivity for the reflected wavelengths using equation (25), we developed a MATLAB program that performs ray tracing. The results showed that the reflectivity of light from an amorphous silicon solar cell is approximately 0.25.

Practical Situation of Solar Cells for One-Dimensional Grooves:

In this section, we studied the effect of geometry on the performance of amorphous solar cells under laboratory conditions. However, the path of the beam will certainly be affected when the solar panel is placed in its natural position, as it will be influenced by the sun's inclination angle and the angles of sunrise and sunset, which change throughout the day. Therefore, it was necessary to study the central and local solar coordinates and understand their parameters. [11]. The solar radiation falling on the solar panel is decomposed into two components: one directed parallel to the groove edge and the other perpendicular to the groove edge, both of which lie parallel to the plane of the panel. To track the path of the solar beam, we must consider both the hour angles (H) and the inclination angles (D). The angle between the incident beam and the vertical coordinate represents the azimuth angle (Z). In contrast, the angle between the projection of the incident beam on the east-south plane and the east direction represents the hour angle (H). We found the relationship between the incident ray, the azimuth angle (Z), the plate angles (∅), and the components of the incident rays in Figure 4. Since the sun's rays are oblique, as mentioned earlier, the incident rays are decomposed into two components. The component sin(α) is parallel to the edge of the groove, and its effect is neglected in the case of one-dimensional grooves. The other component, cos(α), is the one that will be taken into consideration in the case of one-dimensional grooves.

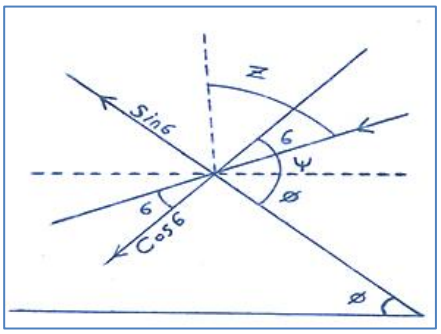

Fig. 4: The relationship between the incident ray and both the azimuth and plate angles[6].

We found theoretically in Figure 4 the sum of angles (ψ) and (Z) is:

$$\psi + Z = 90 \quad \ldots (26)$$

So it is:

$$\psi = 90 - Z \quad \ldots (27)$$

In Figure 5, we can observe that:

$$\psi + \sigma + \phi = 90 \quad \ldots (28)$$

Where σ represents the angle between the incident ray on the plate and the plate's normal, after

DOI:https://doi.org/10.25130/tjps.v31i1.1878

equating equations (27) and (28), the following equation is derived:

$90 - \sigma - \phi = 90 - Z$ … (29)

$\sigma = Z - \phi$ … (30)

Calculation of Photo Current Density for One-Dimensional Groove:

One of the most important quantities to calculate is the light current density (J_P) at any angle of incidence and at any time of day. This depends on the amount of light collected by the groove at a specific hour of the day and for a particular day of the year. Therefore, it is essential to calculate the key angles, including the azimuth angle (Z), the inclination angle (D), and the hour angle (H), as these determine the optimal tilt angle (ϕ) for the solar panel. We chose to perform the calculations during the summer, specifically on July 25th, to determine the optimal tilt angle for the solar panel on that day, since the panel's tilt angle does not change significantly throughout the year.

$\phi = Z_{noon} = (D - L)$ … (31)

The inclination angle of the solar panel is adjusted to align perpendicularly with the sun's rays at noon, maximizing the generated current density. This alignment occurs when the panel's inclination angle matches the azimuth angle at noon, based on the principle that two lines are perpendicular when their angles are 90°.

To determine the complementary angle of inclination, along with the inclination (D), hour (H), and azimuth (Z) angles, we first calculate the number of days elapsed since the vernal equinox (March 21). For July 25, this period spans (126 days). Using this value, we compute the complementary angle of inclination (D) using equation (32) [11], resulting in a value of approximately (70.7410°).

$\cos D = \sin 23.5 \sin \frac{360 \times X_n}{365.25}$ … (32)

The hour angle (H) is calculated using equation (33) for specific times of the day: (9:00, 10:00, 10:30, 11:00, 11:30, and 12:00). At these times, the corresponding values of the hour angle are: (-45°, -30°, -22.5°, -15°, -7.5°, and 0°), respectively. Here, (t) represents the number of hours before or after solar noon, with a negative sign indicating times before solar noon. These calculations are based on the latitude of Mosul, Iraq (36°N)[11].

$H = \pm \frac{360}{24} t$ … (33)

In this context, the complementary angle to the latitude angle (L) is calculated using the equation.

$L = 90 - 36$ … (34)

The azimuth angle (Z) was calculated for the following times of the day (9:00, 10:00, 10:30, 11:00, and 11:30). At this time, the calculated azimuth angle values were (540°).

$\cos Z = \cos D \cos L + \sin D \sin L \cos H$ … (35)

In this context, (L) represents the complementary angle to the observer's latitude. The values of (L) at different times were as follows: (042.88°, 031.22°,025.93°, 021.44°, and 18.010°). At solar noon (12:00 PM), the azimuth angle (Z) was calculated using the appropriate formula, yielding a value of (16.74°).

$\phi = Z_{noon} = (D - L)$ … (36)

(ϕ) denotes the tilt angle of the solar panel. As we move away from solar noon, the azimuth angle gradually increases until it reaches 90°, at which point the sun's rays are parallel to the Earth's surface, approaching sunrise or sunset. Additionally, the meridian angle (A) was calculated for the three trench head angles during the daylight hours under study using the appropriate equation:

$\tan A = \sin D \sin H (\sin D \sin L \cos H - \cos D \sin L)$ … (37)

The illuminated area (X) was calculated according to the following equation:

$X = \cos(i) \times \frac{2E \sin \alpha}{\sin(i+\alpha)} \times \cos(\sigma)$ … (38)

Where I represents the angle of incidence, 2α represents the groove head angle, and σ represents the angle between the incident ray and the line perpendicular to the solar panel's surface. When the angle of incidence exceeds half of the groove angle of the solar panel, the photocurrent density resulting from light reflected from the panel's front face is calculated.

DOI:https://doi.org/10.25130/tjps.v31i1.1878

$$J_{p1} = X \times J_{inJu} \quad \dots (39)$$

Where as J_{inJu} The current density is generated. The light current density resulting from the reflection of light from the first face and falling on the second face can be calculated using the appropriate equation:

$$J_{p2} = X \times J_{inJu} \times \frac{0.25}{0.75} \quad \dots (40)$$

As for the density of the light current resulting from the reflection of light from the second face and falling on the third face:

$$J_{p3} = J_{p2} \times \frac{0.25}{0.75} \quad \dots (41)$$

The density of the resulting photocurrents from all sides is calculated according to the equation:

$$J_{PT1} = \sum J_{pi} \times \sin(90 - Z) \quad \dots (42)$$

Then the total current density J_T is calculated from the equation below

$$J_{r1} = J_{pr1} \times \frac{84}{87} \quad \dots (43)$$

The illuminated part of the left side is calculated as follows:

$$X_l = \alpha - A \quad \dots (44)$$

So the photocurrent density is calculated from the equation:

$$J_{pl} = \sin(X_l) \times J_{inJu} \quad \dots (45)$$

The rays that will fall on the right side of the groove are calculated as follows:

$$X_r = \alpha + A \quad \dots (46)$$

The photocurrent density in this case is calculated from the equation:

$$J_{pr} = \sin(X_r) \times J_{inJu} \times \cos(\sigma) \quad \dots (47)$$

The photocurrent density generated is collected from both sides, as described in equations (45) and (47). The total current density is then calculated using equation (43). Subsequently, current values are plotted against voltage values to determine the resulting power (Pout) and, consequently, the efficiency (η). At noon (12:00 PM), when the sun's rays are perpendicular to the solar panel, the photocurrent density is calculated using the following equations:

$$J_{pr} = 2 \times \sin(\alpha) \quad \dots (48)$$

$$J_{pl} = 2 \times \sin(\alpha) \times \frac{0.25}{0.75} \quad \dots (49)$$

We calculated the total photocurrent density generated from both sides as follows: the total current is determined using equation (43). The energy incident on the solar panel during July is calculated as follows:

$$J_{PT} = J_{pr} + J_{pl} \quad \dots (50)$$

$$p_{inJu} = p_{invJu} + \sin(90 - Z) \quad \dots (51)$$

After calculating the output power p_{out} by determining the area under the current-voltage (I-V) characteristic curve and the incident power for July, the efficiency (η) is computed at each hour of the day under study and at each groove angle using the following equation:

$$\eta = \frac{p_{out}}{p_{in}} \quad \dots (52)$$

The Effect of Texturing on Two-Dimensional Grooves:

Two-dimensional grooves, in the form of a rectangular-based quadrilateral prism, are utilized to harness light rays directed parallel to the groove's edge, an effect unattainable with one-dimensional grooves. Various configurations exist for two-dimensional formations; however, we selected the rectangular-based prism due to manufacturing considerations. As previously noted, when grooves resemble the letter (V), the solar cell is formed by shaping the ground. Consequently, this two-dimensional configuration is fabricated using straightforward mechanical processes, such as placing vertical rectangular strips on the solar panel's surface. (V)-shaped grooves, incident oblique light decomposes into two components: one, denoted as σ, is significant for one-dimensional groove formations, while the other, cos(σ), is typically neglected. However, because grooves are rectangular prisms, both components are considered in the analysis. The photocurrent density for July is calculated using the following equation:

$$J_{p1} = J_{inJu} \times \sin(\sigma) \times \frac{0.25}{0.27} \quad \dots (53)$$

So the total photocurrent density of the two-dimensional groove is calculated using the following equation:

$$J_{PT2} = J_{p1} \times J_{PT1} \quad \dots (54)$$

DOI:https://doi.org/10.25130/tjps.v31i1.1878

The total light current density obtained for the one-dimensional groove during July is represented by equation (43), from which the total current is calculated. Subsequently, efficiency is determined. This methodology is applied to compute the total current throughout all daylight hours for this groove configuration. At noon (12:00 PM), when the sun's rays are perpendicular to the solar panel, the approach aligns with that used for the one-dimensional V-shaped groove, utilizing equations (48), (49), and (50). The resulting values for light current density, total current, and efficiency are documented for various incident angles and daylight hours during the summer season, covering both one-dimensional and two-dimensional groove formations. For the two-dimensional configuration, specifically grooves shaped as rectangular-based quadrangular prisms, the photocurrent density values are calculated using equations (54) and (45). The corresponding power and efficiency values for July 25 are also determined. These values are presented in Table 1. We find that the energy conversion efficiency is low, and there is no photovoltaic effect due to the poor efficiency of this type of amorphous silicon solar cells. These values change when using non- amorphous silicon solar cells. To compare and determine the maximum photovoltaic efficiency for each groove type analyzed, three grooves were selected, as shown in Tables 2 and 3.

Table 1: The values of the hour, azimuth, and meridian angles, along with the light current, total current, incident and resultant powers, and efficiency during the studied daylight hours for a two-dimensional trough with a vertex angle of 40° in July.

Daylight Hours	$H_\circ$	$Z_\circ$	$A_\circ$	J_P (mA/cm^2)	J_T (mA/cm^2)	p_{in} (Watt/cm^2)	P_{out} (Watt/cm^2)	η
9	45	42.789	79.352	3.012	2.908	0.06604	0.001410	0.021350
10	30	31.217	65.645	6.022	5.814	0.07696	0.002777	0.035992
10.5	22.5	25.927	55.771	8.128	7.848	0.08094	0.003682	0.045490
11	15	21.438	42.291	12.422	11.994	0.08377	0.005468	0.065273
11.5	7.5	18.009	23.510	13.709	13.236	0.08559	0.006020	0.070335
12	0	16.741	0	13.7123	13.230	0.08618	0.006018	0.069830

Table 2: The values of light and total current, incident and resultant power, and efficiency during daylight hours for a two-dimensional groove with a vertex angle of 90° in July.

Daylight Hours	J_P (mA/cm^2)	J_T (mA/cm^2)	p_{in} (Watt/cm^2)	P_{out} (Watt/cm^2)	η
9	4.962	4.791	0.06604	0.002300	0.034827
10	9.220	8.902	0.07696	0.004169	0.054170
10.5	12.036	11.621	0.08094	0.005354	0.066147
11	15.465	14.932	0.08377	0.006904	0.082416
11.5	21.295	20.561	0.08559	0.008980	0.104918
12	28.348	27.371	0.08618	0.011456	0.132931

DOI:https://doi.org/10.25130/tjps.v31i1.1878

Table 3: The values of light and total current, incident and resultant power, and efficiency during daylight hours for a two-dimensional groove with a vertex angle of 110° in July.

Daylight Hours	J_P (mA/cm²)	J_T (mA/cm²)	p_{in} (Watt/cm²)	P_{out} (Watt/cm²)	η
9	4.831	4.664	0.06604	0.002230	0.033764
10	14.133	13.646	0.07696	0.006215	0.080756
10.5	14.489	13.989	0.08094	0.006567	0.081134
11	19.180	18.519	0.08377	0.008686	0.103688
11.5	25.132	24.265	0.08559	0.010310	0.120457
12	32.840	31.708	0.08618	0.012914	0.149849

RESULTS AND DISCUSSION

The resulting power for the three groove head angles was determined using the one-dimensional method previously applied to grooves. Figure 5 illustrates the current-voltage characteristic curves for groove angles of 40°, 90°, and 110°, respectively. From these curves, the resulting power and efficiency were subsequently calculated.

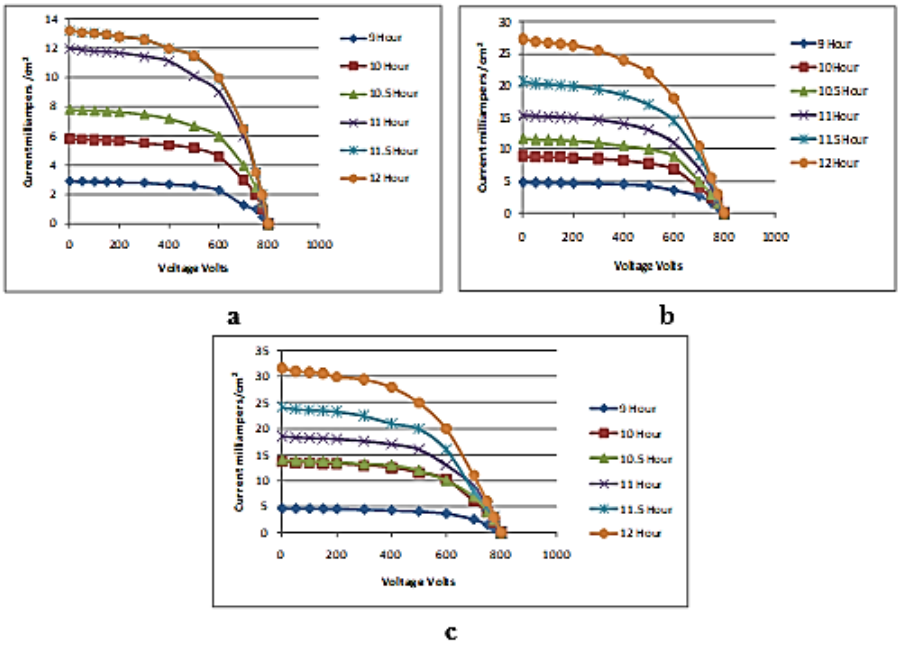

Fig. 5: (a) Current-voltage (I-V) characteristic curves in July for a two-dimensional groove with a vertex angle of (40◦). (b) Current-voltage (I-V) characteristic curves in July for a two-dimensional groove with a vertex angle of (90◦). (c) Current-voltage (I-V) characteristic curves for a two-dimensional groove with a vertex angle of (110◦).

Figure (6) shows the power values obtained for grooves with head angles of (40°, 90°, and 110°) in the form of a rectangular base quadrangular prism. It is observed that at a groove angle of (40°), the obtained power is low at (0.0061 W/cm²), which is less than the power obtained from unshaped cells (0.0086 W/cm²). As the groove head angle increases to 90◦, light trapping improves due to enhanced internal reflections, leading to higher optical absorption and, consequently, increased power output (0.0115 W/cm² at noon), which is higher than the values obtained without shaping and also surpasses those for the one-dimensional groove configuration. For a groove head angle of (110°), internal reflections further enhance absorption, and a maximum power of (0.0129 W/cm²) is attained, which is considered higher than the power obtained without shaping.

DOI:https://doi.org/10.25130/tjps.v31i1.1878

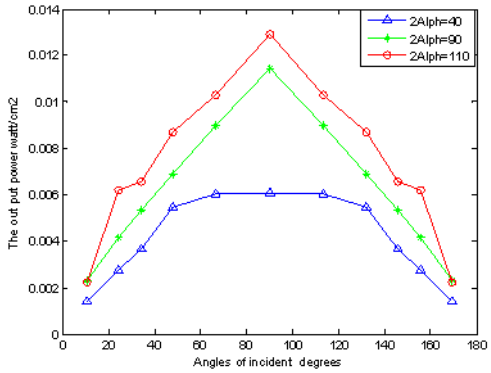

Fig. 6: The change in the resulting power with the angles of incidence for the three grooves of July.

Figure 7 shows the resulting power across daylight hours for the three groove configurations. It is observed that the increase in resulting power values throughout the daylight hours, compared to the one-dimensional configuration, is significant. Specifically, the first and last hours of power dissipation in the one-dimensional formation were utilized.

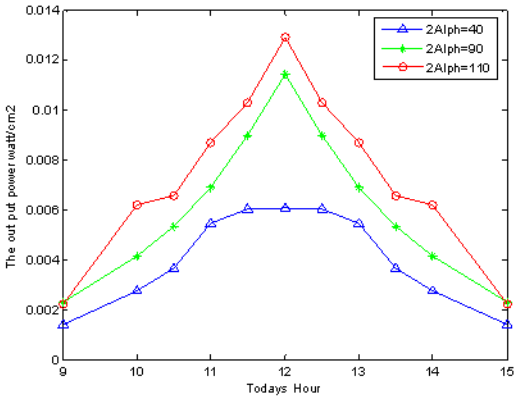

Fig. 7: The resulting power with different daylight hours for the three two-dimensional grooves in July.

Figure 8 shows the efficiency curves for July for grooves with head angles of (40°, 90°, and 110°). At a groove angle of (40°), the efficiency is approximately (6.5 %), spanning an angular range from (50°) to (130°). Increasing the groove head angle to (90°) enhances the efficiency to about (12.5 %), covering an angular range from (70°) to (110°). At a groove angle of (110°), the efficiency reaches a maximum of 14%, with an incidence angle range extending from (50°) to (130°).

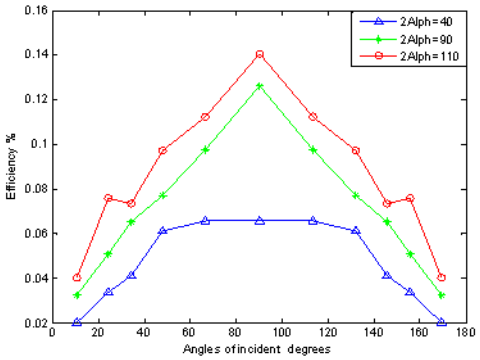

Fig. 8: Change in efficiency with different angles of incidence for a groove in the shape of a prism with a rectangular base.

CONCLUSION

Based on the results obtained theoretically during the study, a groove with a sharp angle (40°) does not significantly enhance efficiency due to increased light reflection losses, resulting in approximately (6.5 %) efficiency. However, increasing the groove head angle to (90°) and further to (110°) results in a significant improvement, achieving maximum efficiencies of (14 %) over a broad range of incidence angles from (50°) to (130°).

Conflict of interest: The authors declared no conflicts of interest.

Sources of funding: This research did not receive any specific grant from funding agencies in the public, commercial, or not-for-profit sectors.

Author contributions: The authors contributed equally to the study.

REFERENCES

1. Salim KD. Studying the effect of light intensity and the dust on the efficiency of a Silicon Solar cell. Tikrit Journal of Pure Science. 2021;26(4):68-70. https://doi.org/10.25130/tjps.v26i4.164

2. Mahmood YH, Atallah FS, Youssef AF. Studying the weather conditions affecting solar panel efficiency. Tikrit Journal of Pure Science. 2020;25(3):98-102. https://doi.org/10.25130/tjps.v25i3.255

3. Salih AR. Optimal Winter and Summer Settings of Solar Photovoltaic Panels for Many

DOI:https://doi.org/10.25130/tjps.v31i1.1878

Locations in the World. Tikrit Journal of Pure Science. 2024;29:6. https://doi.org/10.25130/tjps.v29i6.1691

4. Adamo N, Al-Ansari N, Sissakian VK, Knutsson S, Laue J. Climate change: consequences on Iraq's environment. Journal of earth sciences and geotechnical engineering. 2018;8(3):43-58.

5. Andreani LC, Bozzola A, Kowalczewski P, Liscidini M, Redorici L. Silicon solar cells: toward the efficiency limits. Advances in physics: X. 2019;4(1):1548305. https://doi.org/10.1080/23746149.2018.1548305

6. Mustafa BM. The Effect of Texturing on the Efficiency of a-Si Solar Cell‖. Jou Raf Sci. 2009;20(3):74-89. https://www.iraqoaj.net/iasj/download/95042515c2d00849

7. Green M, Dunlop E, Hohl-Ebinger J, Yoshita M, Kopidakis N, Hao X. Solar cell efficiency tables (version 57). Progress in photovoltaics: research and applications. 2021;29(1):3-15. https://doi.org/10.1002/pip.3371

8. Drechsel J, Männig B, Kozlowski F, Gebeyehu D, Werner A, Koch M, et al. High-efficiency organic solar cells based on single or multiple PIN structures. Thin Solid Films. 2004;451:515-7. https://doi.org/10.1016/j.tsf..2003.11.044

9. Brinker CJ, Lu Y, Sellinger A, Fan H. Evaporation-induced self-assembly: nanostructures made easy. Advanced materials. 1999;11(7):579-85. https://doi.org/10.1002/(SICI)1521-4095(199905)11:7%3C579::AID-ADMA579%3E3.0.CO;2-R

10. Gangwar MS, Agarwal P. Simulation and fabrication of a-Si: H thin-film solar cells: a comparative study of simulation and experimental results. Journal of Materials Science: Materials in Electronics. 2024;35(7):487. http://dx.doi.org/10.1007/s10854-024-12149-8

11. Corkish R, Lipiński W, Patterson RJ. Introduction to Solar Energy. Solar Energy. p. 1-29. https://doi.org/10.1142/9789814689502-0001